Experimental performance and plume characterisation of a miniaturised 50W Hall thruster

IEPC-2019-142

Presented at the 36th International Electric Propulsion Conference
University of Vienna, Austria
September 15-20, 2019

Antonio Gurciullo [*]
Exotrail, Massy, 91300, France

Julien Jarrige [†]
ONERA, Université Paris Saclay, F-91123 Palaiseau, France

Paul Lascombes [‡]
Exotrail, Massy, 91300, France

and

Denis Packan [§]
ONERA, Université Paris Saclay, F-91123 Palaiseau, France

The performance metrics and the plume characteristics of a miniaturised Hall thruster are investigated. The thruster is part of the ExoMG™-nano propulsion platform developed by Exotrail and, during the test campaign, it is operated with a power processing unit prototype. Beam divergence, ion energy distribution, thrust and specific impulse are the primary parameters measured during the investigation. The thrust is directly measured with a pendulum-type thrust balance, while the ion current density and ion energy distribution are measured using electrostatic probes. At about 53 W of total input power and at a total xenon flow rate of 2.7 sccm (anode plus cathode), the thrust, total specific impulse and total efficiency are 2 mN, 800 s and 15 %, respectively. At the same power, the mass utilisation efficiency is about 67 %, the divergence efficiency is 70-75 % and the half-angle where 90 % of the plume ion current is found is 68-72^o. A comparison with other commercially available propulsion platforms is also presented.

Nomenclature

amu	atomic mass unit
CEX	charge-exchange collision
CRP	cathode reference potential
D	distance between the Faraday probe and the thruster exit
DAQ	data acquisition
FEEP	Field Emission Electric Propulsion
g	standard acceleration due to gravity, $= 9.806\,\mathrm{m/s^2}$

[*]Plasma Physics Research Engineer, antonio.gurciullo@exotrail.com.
[†]Research Scientist, Physics and Instrumentation Department, julien.jarrige@onera.fr.
[‡]Chief Scientific Officer, paul.lascombes@exotrail.com.
[§]Research Scientist, Physics and Instrumentation Department, denis.packan@onera.fr.

HT	Hall thruster
$I_{sp,tot}$	total specific impulse
I_{tot}	total ion current
J_i	ion current density
L_i	position (mass leverage) of the mass i
m	ion mass
$\dot{m}_a$	anode mass flow rate
$\dot{m}_c$	cathode mass flow rate
$\dot{m}_i$	ion mass flow rate
M_i	weight of the mass i
PID	Proportional-Integrator-Derivative
PPU	power processing unit
P_{tot}	total input power
RF	radio frequency
RPA	retarding potential analyser
sccm	standard cubic centimetre per minute
T	thrust
T_{eq}	equivalent thrust
V_{PID}	signal of the PID regulator of the balance
Z	charge number

Symbols

η_{tot}	total efficiency
ϕ	rotation angle

I. Introduction

Surveys such as that conducted by SpaceWorks[1,2] and Euroconsult[3] have shown an increase interest in micro- and small-satellites (up to 500 kg) in the recent years. This interest is backed by the progress, cost reduction and standardisation of satellite hardware which, in turn, allow access to on-orbit assets to small companies and research institutions. After an initial success of small-satellites developed by research institutions, more complex civil mission scenarios in which orbital manoeuvres are required, such as orbit transfer and drag compensation, demand the exploitation of propulsion subsystems.

Exotrail enters the small-satellite market by providing, in addition to a mission design software,[4] integrated propulsion systems which include Hall thruster, thermionic cathode, gas delivery system, on-board computer and power processing unit. Two propulsion systems have been developed, the ExoMG^{TM}-nano (50 W thruster) and the ExoMG^{TM}-micro (100 W thruster). ExoMG^{TM}-nano is fully designed by Exotrail, while the design of the ExoMG^{TM}-micro thruster is done in collaboration with ICARE (CNRS) under the partnership ORACLE (from the French labORAtoire Commun propuLsion Electrique).

The primary goal of the research presented here is to experimentally investigate the performance and to determine the plume characteristics of the ExoMG^{TM}-nano thruster head. The thruster head consists of a miniaturised Hall thruster and a thermionic cathode assembled on an interface plate, where the relative position between the thruster and the cathode resembles that used in a flight configuration. Beam divergence, ion energy distribution, thrust and specific impulse are the primary parameters measured during the investigation. The thrust is directly measured with a pendulum-type thrust balance, while the ion current density and ion energy distribution are measured using electrostatic probes.

A secondary goal of this test campaign is to operate the thruster and cathode by means of a power processing unit (PPU) prototype, which is fully controlled by the user. Details on the experimental setup are discussed in the next section.

This manuscript is divided into further four sections. The reader is introduced to the experimental setup in section II and to the test plan in section III. Results and discussion are found in section IV, while section V contains the conclusions.

II. Experimental setup

A. ExoMG^{TM}-nano and thruster head

Figure 1 shows an integrated ExoMG^{TM}-nano during coupling tests. The propulsion system includes an electronics part (PPU and on-board computer), a gas delivery system (Xe tanks, pressure regulator, manifolds and valves) and the thruster head. In this paper, we will focus on the tests performed on the thruster head.

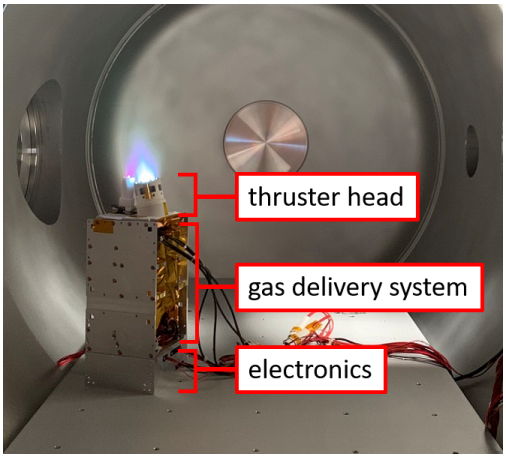

Figure 1: Picture of an assembled ExoMG^{TM}-nano L during coupling tests. The various subsystem locations are highlighted.

The ExoMG^{TM}-nano thruster head consists of a miniaturised Hall thruster and a thermionic cathode

mounted on a metal baseplate. The Hall thruster has been miniaturised according to scaling laws based on physical principles[5,6] and its external diameter is about 3.5 cm. The main components of the Hall thruster are a ceramic channel, an anode and a magnetic circuit with permanent magnets. Due to its small dimensions, the power per unit surface within the channel is higher than that found in larger Hall thrusters and the thermal design has an important role in order to avoid overheating the magnets. During the test campaign here presented, long runs up to one hour have been performed. The total power required for operation (the cathode is self-heated) is between 35 and 70 W.

The cathode consists of a lanthanum hexaboride (LaB_6) insert encapsulated within a metal tube, a heater circuit and a metal keeper. During the ignition phase, the heater provides the power required to reach the emission temperature of the thermionic insert. The emitted electrons are initially extracted by the keeper thanks to an initially applied voltage with respect to the emitter. As soon as the discharge between the emitter and the thruster anode is established, the heater power is reduced to zero and the keeper is allowed to be electrically floating. In addition to facilitate electron extraction, the keeper protects the cathode tube from ion bombardment and reduces the power losses due radiation. Similarly, the ceramic cover reduces the ion bombardment on the keeper and limits the exposure of the keeper to the external plasma. The cathode typically requires less than 50 W of heating power at ignition and less than 0.5 sccm of xenon. Pictures of the thruster head mounted on the thrust balance arm, rotation stage and Faraday probes are shown in figure 2. In the left picture, a gridded Faraday probe and a guarded ring Faraday probe are shown, however, in this paper, only results acquired by the gridded Faraday probe are presented.

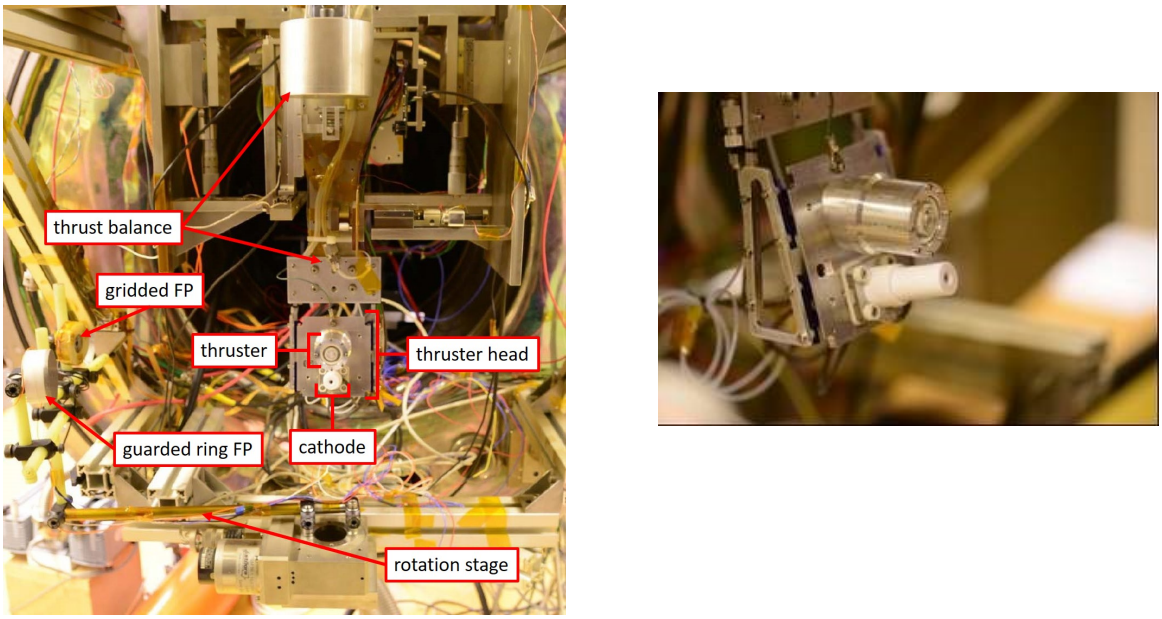

Figure 2: Pictures of the thruster head mounted on the thrust balance at ONERA's facility.

B. Gas delivery system

The anode and the cathode are fed with xenon using external mass flow controllers (Bronkhorst El-Flow) with a full scale of 10 sccm and 4 sccm, respectively.

C. Electrical equipment

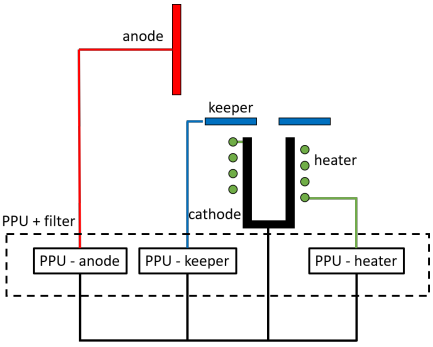

Figure 3: Schematic of the electrical connections between anode, cathode and PPU.

The electrical equipment can be grouped into three categories: (i) power, (ii) data acquisition and (iii) plasma diagnostics. The power electrical equipment includes the PPU, a 12 V and a 20 V power supplies (which feed the PPU), and a filter-and-measure box, whose circuitry filters out the oscillations originated from the plasma discharge. A schematic of the electrical connection between the anode, cathode (which includes keeper, heater and cathode return) and PPU is shown in Fig. 3. The cathode return wire is electrically insulated from the facility ground, thus allowing the measurement of the cathode reference potential (CRP) with respect to the facility ground. During discharge, the keeper is electrically floating with respect to the cathode potential.

The data acquisition system includes (i) a 16-channel 18 bit, 500 kHz National Instrument data acquisition (DAQ-ONERA) board and (ii) seven Keithley digital multimeter DMM6500 whose data are recorded into a PC through a custom LabVIEW script (DAQ-Exotrail). The DAQ-ONERA is dedicated to the acquisition of the thrust balance and plasma diagnostics measurements. In addition to these, the anode voltage, keeper voltage and the CRP are measured by the DAQ-ONERA through voltage dividers; the current through the anode and the cathode lines are measured by means of Hall-effect probes (LEM CTSR 0.3P), whose output voltage (proportional to the current) is also acquired by the DAQ-ONERA (acquisition frequency of 40 Hz). The DAQ-Exotrail acquires the voltage and current of the anode, keeper, heater and CRP at an acquisition frequency of about 1 Hz. It is important to note that the CRP and anode, keeper, heater voltages are measured at the proximity of the thruster head, by-passing the powered lines. This method allows the user to discard the power losses along the powered lines.

A detailed description of the plasma diagnostic configuration is presented in Section III.E.

D. Thrust balance

The thrust balance is a vertical pendulum with a quasi-frictionless pivot, which is described in details in ref.[7] The thruster is mounted at the end of the pendulum arm on which it applies a horizontal force. In the free pendulum mode, the arm then moves from its initial position to a new, tilted equilibrium position, where the torque exerted by the thrust and the torque exerted by the weight of the pendulum arm cancel each other. The angle of the pendulum is then a linear measure of the thrust, given that the angle is usually very small ($\ll 1^o$). Two displacement sensors are placed on the pendulum arm: one is an accelerometer (Honeywell QA 700) for which the axis measures the projection of gravity; the other is a capacitive sensor (Focale MC 900) that measures the linear displacement of the arm. A coil actuator is placed at the bottom of the pendulum. It consists of a permanent magnet fixed on the arm near a planar coil placed on the vacuum tank. When making a current flow through the coil, a force is applied on the arm. Because of the frictionless movement of the coil, and provided that the movement is very small, this force is proportional to the current. Two measurement modes can be used: (i) open loop, as described above, where the pendulum is free to move; (ii) closed loop, where a feedback loop uses the coil actuator to maintain the pendulum at its initial equilibrium position. This mode has one clear advantage: the movement of the pendulum becomes second order. This is important if the movement is perturbed by non-linear flexure phenomena (like plastic deformation of gas tubes and cables), because these effects will be dramatically reduced.

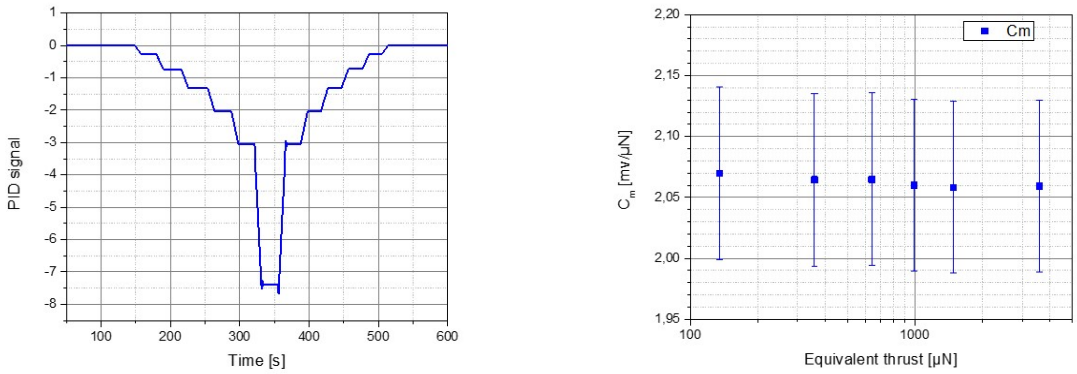

Figure 4: Typical PID signal and calibration coefficient obtained during the calibration procedure.

All thrust measurements performed during this campaign were done in closed loop mode. The current flowing though the coil actuator is controlled with a Proportional-Integrator-Derivative (PID) system. The process variable is the signal of the capacitive sensor, which is fed to the PID controller (SRS SIM960). When the thruster applied a force on the pendulum, the PID output signal is modified, and the resulting magnetic field interacts with the permanent magnet to produce a force. The output voltage from the PID controller is directly proportional to the force applied by the thruster, provided that the error is small enough. The thrust can then be measured from the PID signal, knowing the calibration factor.

One of the advantages of a pendulum balance is that it allows for an absolute and precise thrust calibration. The principle is to deposit masses on a small horizontal arm attached to the pendulum. The weights of the masses are calibrated very precisely with a Mettler Toledo balance precise to 0.01 mg. The masses are placed on a vertical translation stage, and are deposited sequentially on the calibration arm, thus imposing calibrated torques on the balance.

The equivalent thrust T_{eq} for each mass is given by

$$T_{eq} = \frac{L_i M_i g}{L_T} \tag{1}$$

where L_i and M_i are the position (mass leverage) and the weight of the mass i, and L_T is the thruster leverage.

An example of PID signal (after post-processing) recorded during the calibration procedure is shown in figure 8. The calibration coefficient C_m can then be determined as a function of the cumulated equivalent thrust for each mass:

$$C_m = \frac{V_{PID}}{T_{eq}} \tag{2}$$

where V_{PID} is the signal of the PID regulator of the balance. In this example, a mean value of 2.06 mV/µN is found for the balance calibration.

E. Plasma diagnostics

The thrust balance, gridded Faraday probe and the ion energy analyser used to characterise the ExoMG^{TM}-nano thruster are described in the following sections.

1. Gridded Faraday probe

The ion current density is measured with a one-grid Faraday probe. The aperture diameter is 6 mm, and the grid transparency is 50%. The collector of the probe is biased negatively (with respect to the vacuum chamber) in order to repel all incoming electrons. The probe current is taken in the ion saturation zone of the I-V curve (see figure 5a). The floating grid at the entrance of the probe is used to shield the plasma

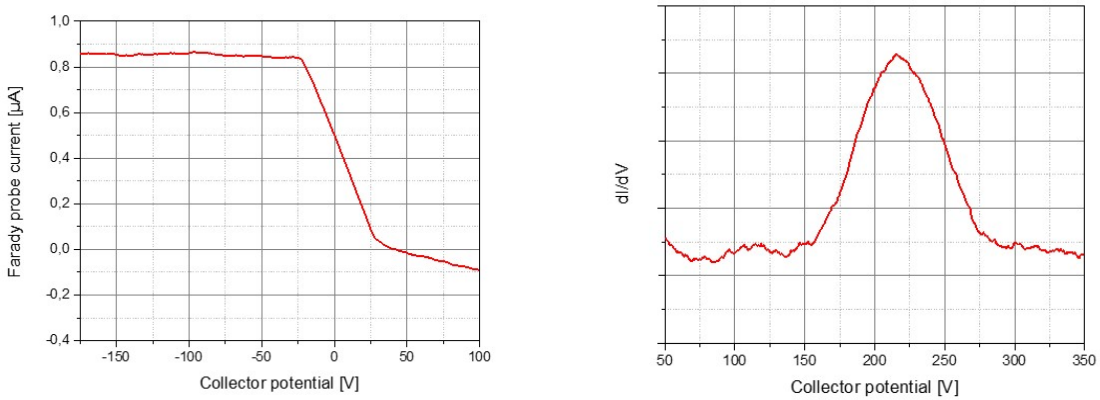

(a) (b)

Figure 5: (a) Example of I-V curve obtained with the Faraday probe. The ion saturation region is reached when the collector is biased below −20 V. (b) Example of the first derivative of an I-V curve taken with Faraday probe current in energy analysis mode. The mean ion energy is about 215 eV.

from the biased collector. The collector is biased using a high voltage power supply (Applied Kilovolt) and the probe current is measured through a shunt resistor.

The one-grid Faraday-probe can also be operated similarly to a retarding potential analyzer (RPA) in order to determine the mean ion energy.[8] The probe is then placed in front of the thruster, with the grid floating, and the collector potential is swept. When the bias voltage of the collector is equal to the beam ion energy, the ions are repelled, and the probe current is suddenly changed. Even though a one-grid RPA is not capable of measuring the full ion energy distribution function (because of high energy electrons passing through the floating grid), the mean ion energy can be inferred from the first derivative of the I-V curve, as can be seen in figure 5b.

The Faraday probe is mounted on a rotation stage, and the distance to the thruster exit is $D = 27\,\text{cm}$. For angular distributions of ion current density, the probe is moved from from 90^o to -90^o. A schematic of the frame of reference of the Faraday probe setup is shown in figure 6.

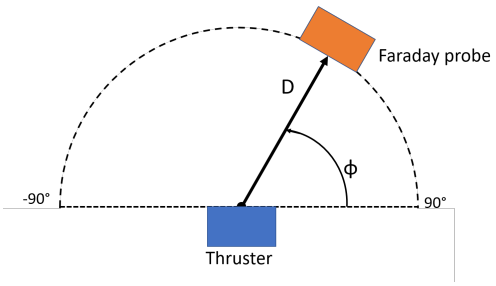

Figure 6: Frame of reference of the Faraday probe.

2. *Ion energy analyser*

The ion energy is also measured with a commercial ion analyzer (Hiden PSM), which can perform scans of energy up to 1000 eV (for a given mass-to-charge ratio, m/Z) and scans of mass up to 300 amu (for a given ion energy). An example of energy distribution function is given in figure 7.

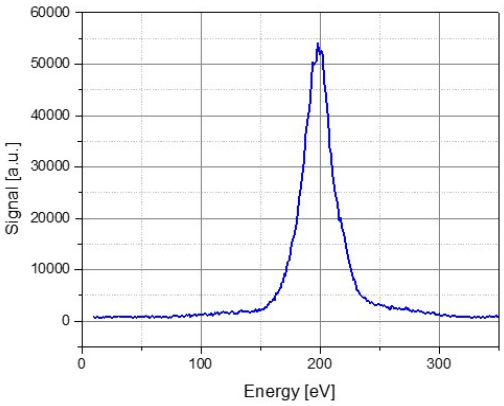

Figure 7: Typical ion energy distribution function measured with Hiden PSM analyzer.

F. Facility

The experiments are performed in B61 vacuum chamber (4 m m long, 1 m in diameter) at ONERA centre of Palaiseau. The secondary pumping consists of a turbomolecular pump (2000 L/s for N_2) and a cryogenic pump (8000 L/s for xenon). The base pressure is around 10^{-6} mbar. The background pressure during the tests is measured with a cold cathode gauge (Pfeiffer Compact Full Range). In the conditions of the experiments (total xenon flow rates between 2.5 and 3.8 sccm), the background pressure is below $3 \cdot 10^{-5}$ mbar (N_2 pressure).

III. Test plan and performance metrics

The test plan consists on a sequence of events that take the following order. First, the cathode is heated by increasing the heater current. In both anode and cathode gas line, a fixed gas flow is maintained. Second, the main plasma discharge is initiated by switching off the heater and then biasing the anode potential. The discharge parameters (voltages and currents) are monitored in order to estimate a stable operation point. Generally, the discharge parameters are constant after 6-9 minutes from ignition. Due to the number of operational points to be tested, it has not been possible to wait for thermal equilibrium of the overall structure (a PT100 sensor is placed on the baseplate). However, long runs, up to one hour, have been also characterised. After the discharge reaches stability, angular scans of the ion current density are performed with the Faraday probe, and the ion energy distribution function is analyzed along the axis of symmetry of the thruster using the ion analyzer and the Faraday probe. As the last event, the anode voltage is voluntary switched off in order to directly measure the thrust by means of the thrust stand. The thrust data are usually taken 10-15 minutes after ignition. The cathode xenon flow rate is maintained at 0.3 sccm throughout the tests. The thruster performances are explored within a xenon flow rate range of $[2.2, 2.8]$ sccm and various anode voltages, such that the investigated total power range is $[37, 61]$ W. It is important to note that the power input to the thruster head delivered from the PPU takes into account the total power deposited in the cathode, which is self-heated, and into the anode discharge (ionisation, various losses and ion acceleration).

The performance metrics discussed in the following sections are here defined. The total specific impulse is

$$I_{sp,tot} = \frac{T}{(\dot{m}_a + \dot{m}_c)\, g} \tag{3}$$

where T is the thrust measured by the thrust balance, $\dot{m}_a$ and $\dot{m}_c$ are the anode and cathode mass flow rates, respectively, and $g = 9.806\,\mathrm{m/s^2}$ is the standard acceleration due to gravity.

The total efficiency is defined as

$$\eta_{tot} = \frac{T^2}{2\,(\dot{m}_a + \dot{m}_c)\, P_{tot}} \tag{4}$$

where P_{tot} is the total input power.

The total ion current, computed from the Faraday probe data, is calculated as

$$I_{tot} = \pi D^2 \int_{-90^o}^{90^o} J_i(\phi) \sin(\phi) d\phi \tag{5}$$

where $J_i(\phi)$ is the ion current density as a function of the rotation angle ϕ and D is the distance between the thruster exit and the Faraday probe. The mass utilisation efficiency and the divergence efficiency are defined as, respectively,

$$\eta_m = \frac{\dot{m}_i}{\dot{m}_a + \dot{m}_c} \tag{6}$$

and

$$\eta_d = \frac{\int_{-90^o}^{90^o} J_i(\phi) \cos(\phi) \sin(\phi) d\phi}{\int_{-90^o}^{90^o} J_i(\phi) \sin(\phi) d\phi} \tag{7}$$

where $\dot{m}_i$ is the ion mass flow rate.

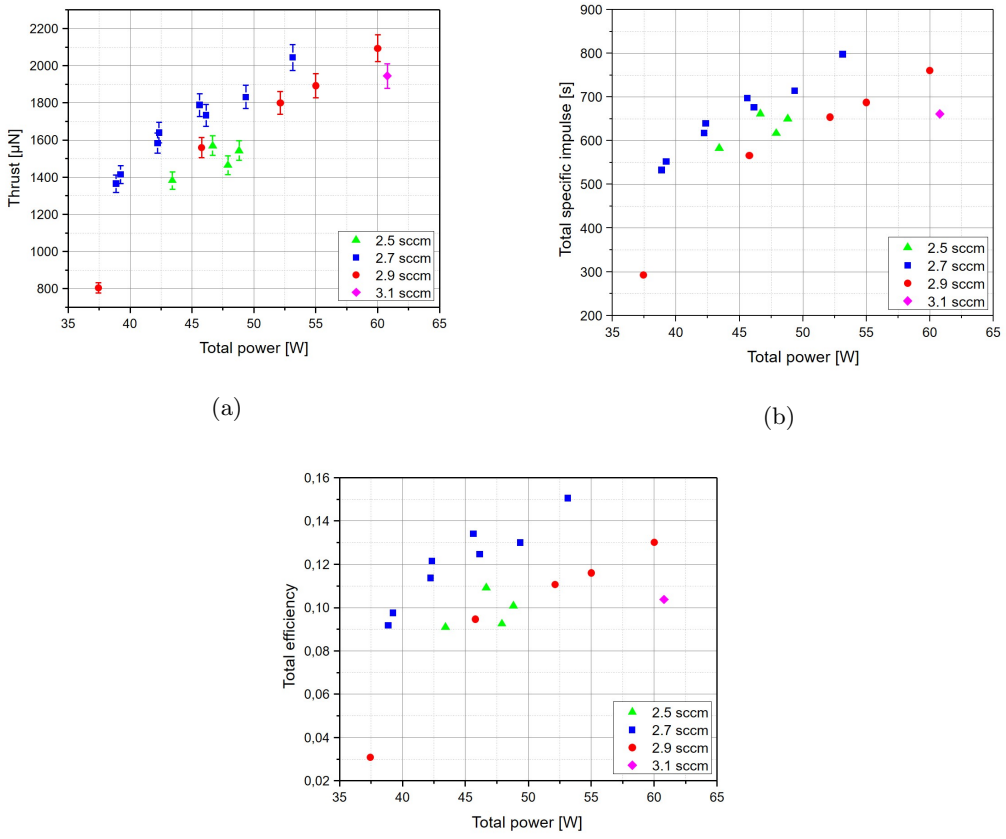

Figure 8: (a) Thrust, (b) total specific impulse and (c) total efficiency as functions of total input power at various total gas flow rates (anode plus cathode).

IV. Results and discussions

In this section we present and discuss the experimental performance of the ExoMG^{TM}-nano thruster. First, thrust, total impulse and total efficiency are presented. Then the ion plume characteristics are shown, such as angular distribution of the ion current density, mass utilisation, divergence efficiency, divergence angle and ion energy distribution along the thruster axis of symmetry.

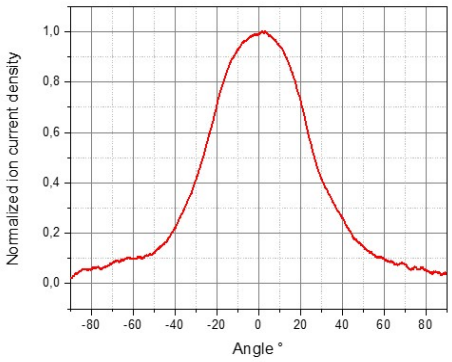

Figure 9: Example of angular distribution of the ion current density at a total power of 53.1 W and total gas flow rate of 2.7 sccm.

A. Thrust, total specific impulse and total efficiency

Figures 8a, 8b and 8c show the thrust, total specific impulse and total efficiency as functions of the total input power at various total gas flow rates (anode plus cathode), respectively. In general, the performance metrics tends to increase with power. Within the explored power and gas flow ranges, the thrust varies from 0.8 to 2.1 mN and the highest thrust has been measured at 60 W at a total flow rate of 3.1 sccm. The total specific impulse and total efficiency are in the range of $[300, 800]$ s and $[3, 15]$ %, respectively. The most performing condition, suitable for a small satellite, is at about 53 W of total input power and at a gas flow of 2.7 sccm, where the thrust, total specific impulse and total efficiency are 2 mN, 800 s and 15 %, respectively. Still at 2.7 sccm, the thrust can be throttle from 1.4 mN to 2 mN when the input power is swept from 38 W to 53 W. At these conditions the total specific impulse varies from 530 s to 800 s and the total efficiency from 9 % to 15 %.

B. Plume characteristics

An example of the angular distribution of the ion current density is shown in figure 9. The post-process analysis does not take into account the effect of charge-exchange collisions (CEX) between fast ions and background neutrals, which has been shown to influence the tails and peak of the ion current density angular distribution of Hall thrusters.[9] Namely, the CEX collisions with the background neutral population increase the divergence of the plume. This effect can be mitigated by lowering the background pressure during plume characterisation. During tests, the typical background pressure is below that recommended by Dankanich *et al.*[10] for plume measurement and performance characterisation.

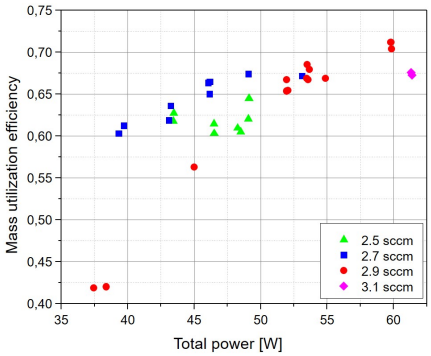

Figure 10: Mass utilisation efficiency as a function of the total power at different xenon flow rates.

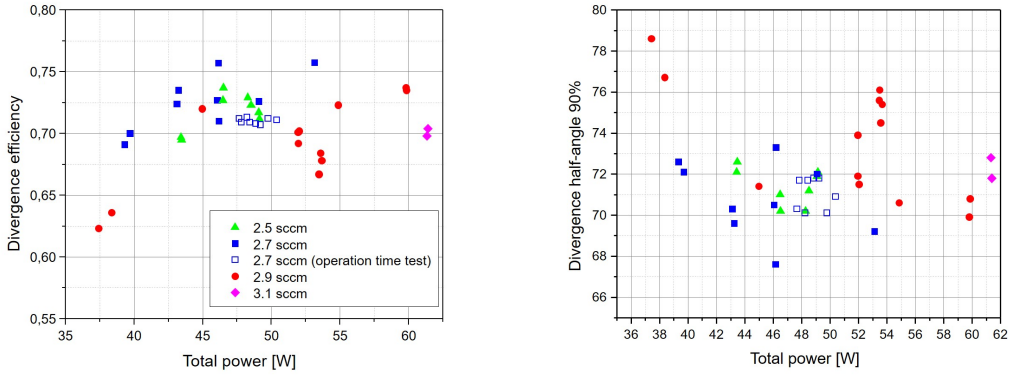

(a) (b)

Figure 11: (a) Divergence efficiency and (b) divergence half-angle $\theta_{90\%}$ as functions of total input power at various total gas flow rates (anode plus cathode).

Figure 10 shows the mass utilisation efficiency as a function of the total power at different gas flow rates. The mass utilisation efficiency tends to increase with the discharge power and the highest efficiency is 71 % at 60 W and 2.9 sccm. At 53 W and 2.7 sccm, the mass utilisation efficiency is about 67 %.

The divergence efficiency and the divergence half-angle $\theta_{90\%}$ as functions of total input power at various total gas flow rates are shown in figure 11. The divergence efficiency slightly increases within the power range investigated and, at the same time, the divergence half-angle slightly decreases. At a xenon flow rate of 2.7 sccm and a power of about 50 W, the divergence efficiency and half-angle are 70-75 % and 68-72^o, respectively. In figure 11 the plume characteristics at 2.7 sccm have been monitored to up 40 minutes of continuous operation (empty blue square). As the discharge duration increases the total power decreased, but the plume divergence characteristics remain constant.

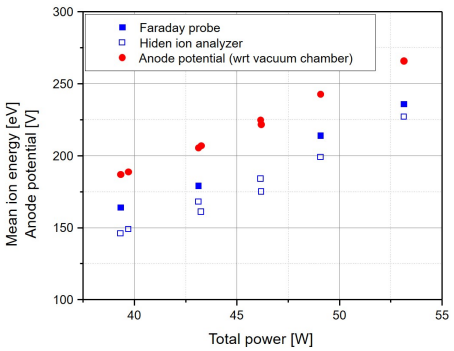

Figure 12: Mean ion energy and anode potential (with respect to the facility ground) as functions of the total power.

Figure 12 shows the mean ion energy and anode potential (with respect to the facility ground) as function of the total power. The results of the gridded Faraday probe and the ion analyser are in line – the mean ion energy estimated by the Faraday probe are systematically lower than those acquired with the ion analyser. In general, the mean ion energy increases with the input power (due to an increase of the anode voltage) and is about 40 eV below the anode potential.

As mentioned above, the plasma plume characteristics have also been measured as functions of the thruster operation time. In particular, the normalised total ion current and the mean ion energy as function of the operation time are shown in figure 13. The data are recorded at constant anode voltage and total

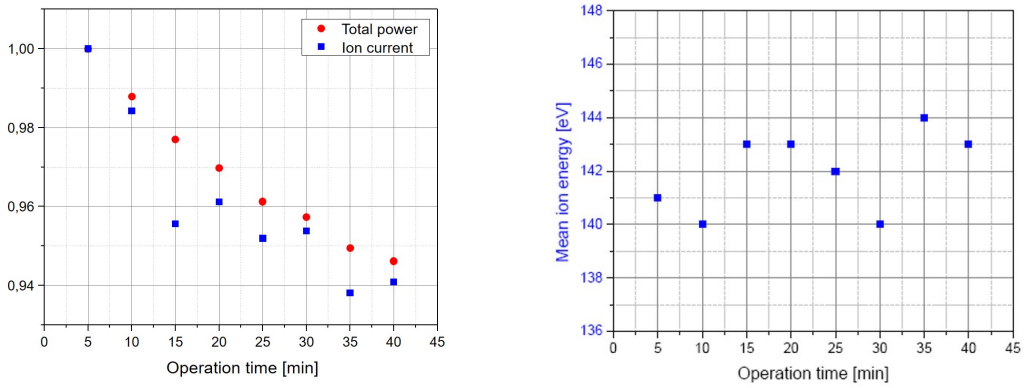

(a) (b)

Figure 13: (a) Normalised total ion current and total power and (b) mean ion energy as functions of the thruster operating time.

xenon flow rate. As seen in figure 13a, the total power (red circles) and the ion current (blue squares) decrease by 5-6% between 5 and 40 minutes of operation time. Post-test inspections led us to believe that this is a consequence of the thruster structure heating over time which impacted the gas delivery pipe of the test setup (causing xenon leaks). On the other hand, the mean ion energy is constant throughout the discharge (see figure 13b).

C. Comparison with other thrusters

A comparison of some of the electric propulsion thruster technologies for low-power small-satellite applications, whose performance metrics are publicly available (data are taken from last published literature or official websites), is shown if table 1. At a given input power, the Hall thruster (HT) technology achieves higher thrust among the technologies here compared. On the other hand, the HT specific impulse resides in the medium-low range when benchmarked against the other technologies.

Table 1: Comparison of various electric propulsion technologies for small satellites.

Technology	Thrust [µN]	Specific impulse [s]	Power [W]	Total efficiency [%]
FEEP[11]	350	4200	40	18%
HT (Exotrail)	**2050**	**800**	**53**	**15.1%**
RF[12]	600	150	50	0.9%
RF[13]	850	850	55	6.4%
RF-ion[14]	1000	1000	60	8.2%

V. Conclusions

The thruster head of the ExoMG^{TM}-nano propulsion platform has been experimentally characterised while operated with a PPU prototype. The thruster head consists of a miniaturised Hall thruster and a thermionic cathode mounted on a metal baseplate. The tests have been performed at ONERAs facility in Palaiseau and the diagnostic tools include a thrust balance, a one-grid Faraday probe and a commercial ion energy analyser. Beam divergence, ion energy distribution, thrust and specific impulse are the primary parameters measured during the investigation. The thrust is directly measured with a pendulum-type thrust

balance, while the ion current density and ion energy distribution are measured using electrostatic probes. At about 53 W of total input power and at a total xenon flow rate of 2.7 sccm, the thrust, total specific impulse and total efficiency are 2 mN, 800 s and 15 %, respectively. At the same power, the mass utilisation efficiency is about 67 %, the divergence efficiency is 70-75 % and the half-angle where 90 % of the plume ion current is found is 68-72^o. A comparison among other thruster technologies for small satellites confirms that HTs are suitable for missions that require high thrust.

Acknowledgments

This work was supported by the French Ministère de l'Enseignement supérieur, de la Recherche et de l'Innovation, the Secrétariat Général pour l'Investissement and Bpifrance under the Grand Prix i-Lab 2018 and the Concours d'Innovation 2019 programs. Antonio G. and Paul L. would also like to thank Exotrail's team for the invaluable technical support along this test campaign.

References

[1]SpaceWorks, "SpaceWorks - Nano Microsatellite Market Forecast 9th Edition 2019," 2018.

[2]SpaceWorks, "SpaceWorks - Forecast 8th Edition 2018," 2019.

[3]Euroconsult, "Prospects for the Small Satellite Market," tech. rep., 2018.

[4]P. Lascombes, A. Fiorentino, and P. Dewost, "Electric Propulsion for Small Satellites. A case study," in *36th International Electric Propulsion Conference*, no. 15-20 September, (Vienna, Austria), pp. IEPC–2019–418, 2019.

[5]V. Khayms, *Design of a Miniaturized Hall Thruster for Microsatellites*. Master of science in aeronautics & astronautics, Massachusetts Institute of Technology, 1997.

[6]F. Battista, E. A. De Marco, T. Misuri, and M. Andrenucci, "A Review of the Hall Thruster Scaling Methodology," in *30th International Electric Propulsion Conference*, no. 17-20 September, (Florence, Italy), 2007.

[7]T. Vialis, J. Jarrige, A. Aanesland, and D. Packan, "Direct thrust measurement of an electron cyclotron resonance plasma thruster," *Journal of Propulsion and Power*, vol. 34, no. 5, pp. 1323–1333, 2018.

[8]T. Lafleur, F. Cannat, J. Jarrige, P. Q. Elias, and D. Packan, "Electron dynamics and ion acceleration in expanding-plasma thrusters," *Plasma Sources Science and Technology*, vol. 24, no. 6, p. 65013, 2015.

[9]D. L. Brown, M. L. R. Walker, J. Szabo, W. Huang, and J. E. Foster, "Recommended Practice for Use of Faraday Probes in Electric Propulsion Testing," *Journal of Propulsion and Power*, vol. 33, no. 3, pp. 582–613, 2017.

[10]J. W. Dankanich, M. Walker, M. W. Swiatek, and J. T. Yim, "Recommended Practice for Pressure Measurement and Calculation of Effective Pumping Speed in Electric Propulsion Testing," *Journal of Propulsion and Power*, vol. 33, no. 3, pp. 668–680, 2016.

[11]"Enpulsion website," www.enpulsion.com, [Accessed 2019-09-12], 2019.

[12]M. U. Siddiqui and C. Cretel, "Updated performance measurements and analysis of the phase four RF thruster," in *2018 Joint Propulsion Conference*, no. 9-11 July, 2018.

[13]M. Manente, F. Trezzolani, M. Magarotto, E. Fantino, A. Selmo, N. Bellomo, E. Toson, and D. Pavarin, "REGULUS: A propulsion platform to boost small satellite missions," *Acta Astronautica*, vol. 157, no. June, pp. 241–249, 2019.

[14]J. Martinez, D. Rafalskyi, and A. Aanesland, "Development and Testing of the NPT30-I2 Iodine Ion Thruster," *36th International Electric Propulsion Conference*, no. 15-20 September, pp. IEPC–2019–811, 2019.